

# Topology optimization of variable thickness Reissner-Mindlin plate using multiple in-plate bi-directional functionally graded materials

Nam G. Luu<sup>1a</sup>, and Thanh T. Banh<sup>\*2</sup>

<sup>1</sup>Faculty of Information Technology, Industrial University of Ho Chi Minh city, Ho Chi Minh city 70000, Vietnam

<sup>2</sup>Department of Architectural Engineering, Sejong University, Seoul 05006, Republic of Korea

**Abstract.** This paper firstly presents an implementation of multi-material topology optimization (MTO) for in-plane bi-directional functionally graded (IBFG) non-uniform thickness Reissner-Mindlin plates. The mathematical formulation of the MTO is associated with a first shear deformation theory (FSDT) to solve the minimization of compliance as the objective function. From a multi-phase TO problem with multi-volume fraction constraints, the problem is transferred into many binary phases TO sub-problems with only one volume fraction constraint using an alternating active-phase algorithm in conjunction with the block Gauss-Seidel method. In the study's scope, IBFG materials following effective local bulk and shear modulus are considered to show a more accurate interaction of materials. Besides, the numerical technique of the well-established mixed interpolation of tensorial components 4-node elements (MITC4) is utilized to overcome the shear locking problem occurring to thin plate models. The study formulates in great detailed mathematical expressions for IBFG plates MTO. Several numerical examples of IBFG plates are presented to verify the efficiency and reliability of the current methodology.

**Keywords:** multi-material; topology optimization; variable thickness; in-plate bi-dimensional functionally graded material; FSDT; shear locking phenomenon

---

## 1. Introduction

Functionally graded material (FGM) is a kind of advanced material that is often fabricated by at least two distinct constituents, namely ceramic and metal, with continuously varied material properties in a particular spatial direction. FGM was first discovered in the mid-1980s in Japan to prepare thermal barrier materials to reduce failures caused by the discontinuities of strain and stress fields Koizumi (1997). The FGMs merit consideration as a priority choice in structural applications due to their outstanding advantages produced from the synergy. Indeed, the ceramic withstands the action or effect of high-temperature environments, while the metal works remarkably fracture toughness. Thus, the ceramic-metal composite can eliminate undesired stresses discontinuity appearing in layers of laminated composites. Accordingly, many research papers on using this advanced material have been intensively published (Ebrahimi and Salari 2015, Şimşek and Al-shujairibc 2017, Mantari et al. 2016, Fares et al. 2015, Panyatong et al. 2016, Phung et al. 2014, Nguyen et al. 2014, Mehralian and Beni 2016, Sofiyev et al. 2017) and extensively applied to various engineering areas such as aerospace, aircraft, nuclear plants and high-speed vehicles and so on.

Nemat-Alla (2003) presents a temperature distribution in advanced machines of modern aerospace shuttles and craft to withstand super high temperatures and reduce thermal stresses in terms of uni-directional FG material. After that, an exact three-dimensional solution for free and forced vibrations of uni-directional FG rectangular plates is proposed by Vel et al. (2004), which use

---

\*Corresponding author, Professor, E-mail: btthanhk11@gmail.com

<sup>a</sup> E-mail: luugiangnam.math@gmail.com

a power-law form to vary the material properties along with the plate thickness only. Although uni-directional FGMs have been widely used, such approaches with identical distributions in all outer surfaces might not be perfectly efficient for design structures performing in harsh environments, such as in two or three directional temperature distribution areas. Accordingly, bi-directional FG (bi-FG) materials might be more effective in severe environments to save their weight, even for ones with variable thickness. Therefore, numerous remarkable papers concerning the material distribution optimization of bi-FG materials have been conducted by many researchers in recent years for two-dimensional elasticity problems. For instance, Tanaka et al. (1993a, 1993b, 1996) present a novel methodology for thermoelastic material design bi-FG material to reduce the thermoelastic thermal stress problems. Then, many papers about thermal bi-FG materials can be found in Turteltaub (2002a, 2002b), Cho and Ha (2002), Chen and Tong (2004, 2005), Goupee and Vel (2006). Şimşek (2015, 2016) analyzed the free, forced vibration, and buckling responses of bi-FG Timoshenko beams by using trial shapes expressed in polynomial functions to approximate the generalized beam displacements. Besides the research efforts on bi-FG beam structures as introduced above, in recent years, many researchers have concentrated on the behavior analyses of FG plates with in-plane material inhomogeneity. Xiang et al. (2014) present a 3D approach based on the scaled boundary finite element method to study free vibration and buckling responses of FG plates, while Amirpour et al. (2016) propose an analytical solution for elastic bending deformations of FG plates by using the HSDT including stretching effects in conjunction with the Navier method. Van Do et al. (2017) analyzed bending and buckling analyses of IBFG plates using the FEM and a novel third-order shear deformation theory (TSDT). Several related studies considering the effect of variable thickness on responses of plates and shells using IBFG could be found in Ebrahimi and Najafizadeh (2014), Jalali et al. (2010), Tajeddini et al. (2011), Eftekhari and Jafari (2013), Rajagopal and Hodges (2015), Shufrin and Eisenberger (2016), Baccocchi et al. (2016), Javed et al. (2016), Zur. (2016), and Thang et al. (2016).

In recent years, topology optimization has made remarkable progress as a creative numerical and design methodology, drawing an enormous amount of attention from scientific and engineering communities since the pioneering research by Bendsøe and Kikuchi (1988). Accordingly, many research papers on structural topology optimization (TO) have been intensively published, for instance, Xu et al. 2012, Rozvany et al. 2002, Vatanabe et al. 2016, Roodsarabi et al. 2016, Bagherinejad and Haghollahi 2018. Multi-material topology optimization (MTO) is one of the most interesting issues based on the main ideas of the standard topology optimization field. Multi-material application gives a significant opportunity to add stiffer materials with the same amount of volume constraint with the same goal of single material consideration with respect to achieving both higher structural stiffness and material cost savings. The TO results will always be physically feasible and do not need to be classified in material groups anymore; therefore, it has been solved with a typical single material TO approach (Bendsøe 1995). Then, the three-phase topology optimization method for the design of materials with the extreme thermal expansion is presented Sigmund and Torquato (1997). In this work, the TO method finds the distribution of material phases that optimizes an objective function (e.g., thermoelastic properties) subject to certain constraints, such as elastic symmetry of volume fractions of the constituent phases, within a periodic base cell. The numerical homogenization method based on a finite-element discretization of the base cell utilizes to find the effective properties of the material structure. A method for the MTO with a generalized Cahn-Hilliard model is presented by Zhou and Wang (2007) to define a thermodynamic model, taking into account the bulk energy and interface energy of the phases and the elastic strain energy of the structure. However, one of the difficult issues of MTO is computational time. Therefore, to create

high-resolution optimized designs with a lower computational cost, Lieu and Lee (2017) proposed a novel multi-resolution scheme to perform the MTO in the framework of isogeometric analysis (IGA). Doan and Lee (2017) treated removal of spurious buckling modes which occur in MTO designs for multiple steel materials. Nguyen et al. (2018) proposed TO computation of multi-materials CFRP for retrofitting the concrete beam-column joint with various cases of crack patterns by using multiple materials. Goo et al. (2016) present TO for thin plate structures with bending stress constraints to discover the multi-material design distribution for platelike structures. For Mindlin-Reissner plate structures, a novel resizing algorithm of topology optimization is studied by Belblidiaa et al. (2001), while El-Sabbagh et al. (2008) investigated optimal topologies of plates with various periodic configurations. Luo and Tong (2017) present a novel deformation mechanism-based material model for topology optimization of laminated plates and shells considering large displacements while a Kirchhoff-Love thin plate with multi-directional variable thickness applied for MTO is proposed by Banh and Lee (2019). To eliminate the shear locking phenomenon in Mindlin-Reissner plate theory, when plates are modeled by deformable shear elements, the mixed interpolation of tensorial components for 4-node elements (MITC4) scheme (Bathe and Dvorkin 1985) is utilized. In addition, the Winkler foundation parameter (Kobayashi and Sonoda 1989) is investigated the influence of variable thickness in multi-material optimal topological results by Banh et al. (2020).

Obviously, in most of the afore-cited work, no reports have been published relating to bending MTO of IBFG plates with variable thickness using the FSDT-based MITC4 so far. Therefore, this study is carried out as the first effort. The variable thickness is assumed to continuously change in the x- y- plane by specific functions. Also, to deal with the shear locking phenomenon, a MITC4 is applied to the FSDT plate theory in this article. Besides the rule of mixture, the Mori-Tanaka technique is used to homogenize the material properties of IBFG plates. Additionally, a shear correction factor is considered for the FSDT plate theory to show the shear deformation accurately. Numerical examples are presented to examine the effects of a number of materials in MTO, variable thickness, material gradation, and different boundary conditions on the bending behavior of IBFG plates.

The rest of this article is outlined as follows. The following section exhibits the theoretical formulation of modeling IBFG plates with variable thickness using the FSDT plate theory with the weak form. The finite element model based on the FSDT with MITC4 and the MTO problem statement are elaborately derived in Section 3. Section 4 demonstrates several numerical examples. Finally, Section 5 ends this paper with concluding remarks.

## 2. Theoretical formulation

### 2.1 Constitutive formulation

Let us consider a Reissner-Mindlin plate having a multi-directional variable thickness assumed  $h = h(x, y) = h_0 \lambda(x, y)$  (Banh *et al.* 2020), where  $h_0$  is a minimum value of thickness that can be achieved and  $\lambda = \lambda(x, y)$  is not less than 1 as shown in Fig. 1. The governing equation for in-plane displacements of an arbitrary point located at  $(x, y, z)$  in the plate are given as follow

$$u(x, y, z) = z\phi_x(x, y) \quad (1a)$$

$v(x, y, z) = z\phi_y(x, y)$	(1b)
$w(x, y, z) = w_0(x, y)$	(1c)

where  $w_0$  is displacements of the centroidal line of the plate as shown in Fig.2.  $\phi_x$  and  $\phi_y$  are the section rotations in the  $x - z$  and  $y - z$  planes, respectively.

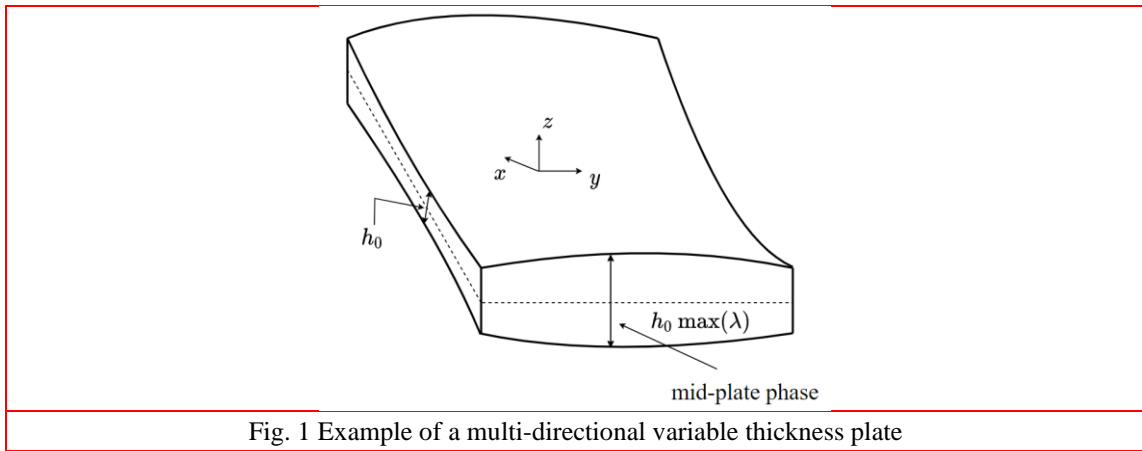


Fig. 1 Example of a multi-directional variable thickness plate

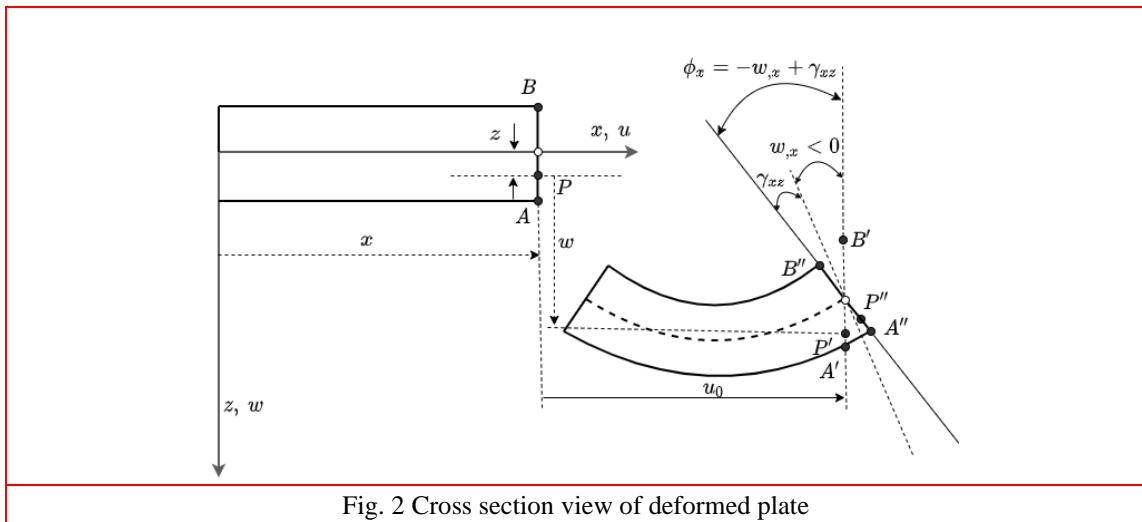


Fig. 2 Cross section view of deformed plate

## 2.2 Geometrical description

The plate is made of functionally graded materials constituted by a mixture of ceramic and metallic components. Through the influence in two in-plane bi-directions of elastic material

properties according to volume fractions of constituents, a power-law distribution of material properties, which is commonly used to describe the variation of material properties, can be expressed as

$$\mathfrak{M} = (\mathfrak{M}_1 - \mathfrak{M}_2) \left(\frac{x}{a}\right)^{k_x} \left(\frac{y}{b}\right)^{k_y} + \mathfrak{M}_2 \quad (2)$$

where  $a$ ,  $b$  and  $h$  are the length, width, and thickness of the plate, respectively;  $k_x$  and  $k_y$  present the power indexes in the  $x$ - and  $y$ - axis, respectively.  $\mathfrak{M}_1$  and  $\mathfrak{M}_2$  stand for the properties of the first and second materials, respectively. However, the interactions between two constituents are not considered by the rule of mixture result as pointed out in refs. (Senthil and Batra 2004, Qian *et al.* 2004), this study utilized the Mori-Tanaka scheme (Mori and Tanaka 1973) in this study to capture these interactions, as shown in Fig. 3, as follow

$$E(x, y) = \frac{9\mathfrak{B}_{\text{eff}} \mathfrak{G}_{\text{eff}}}{3\mathfrak{B}_{\text{eff}} + \mathfrak{G}_{\text{eff}}}, \nu(x, y) = \frac{3\mathfrak{B}_{\text{eff}} - 2\mathfrak{G}_{\text{eff}}}{2(3\mathfrak{B}_{\text{eff}} + \mathfrak{G}_{\text{eff}})} \quad (3)$$

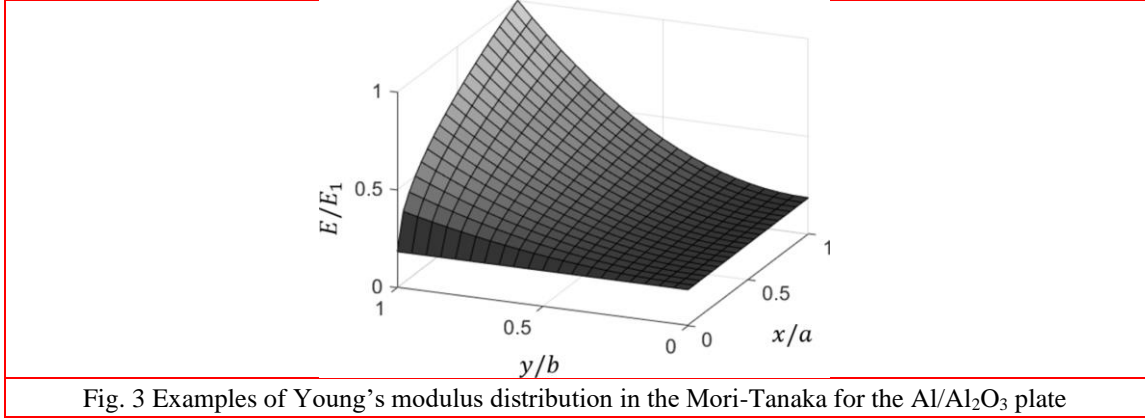
where the effective bulk  $\mathfrak{B}_{\text{eff}}$  and shear modulus  $\mathfrak{G}_{\text{eff}}$  can be expressed by

$$\mathfrak{B}_{\text{eff}}(x, y) = \frac{\left(\frac{x}{a}\right)^{k_x} \left(\frac{y}{b}\right)^{k_y} (\mathfrak{B}_1 - \mathfrak{B}_2)}{1 + \left(1 - \left(\frac{x}{a}\right)^{k_x} \left(\frac{y}{b}\right)^{k_y}\right) \frac{\mathfrak{B}_1 - \mathfrak{B}_2}{\mathfrak{B}_2 + \frac{4}{3}\mathfrak{G}_2}} + \mathfrak{B}_2, \quad (4a)$$

$$\mathfrak{G}_{\text{eff}}(x, y) = \frac{\left(\frac{x}{a}\right)^{k_x} \left(\frac{y}{b}\right)^{k_y} (\mathfrak{G}_1 - \mathfrak{G}_2)}{1 + \left(1 - \left(\frac{x}{a}\right)^{k_x} \left(\frac{y}{b}\right)^{k_y}\right) \frac{\mathfrak{G}_1 - \mathfrak{G}_2}{\mathfrak{G}_2 + \frac{\mathfrak{G}_2(9\mathfrak{B}_2 + 8\mathfrak{G}_2)}{6(\mathfrak{B}_2 + 2\mathfrak{G}_2)}}} + \mathfrak{G}_2 \quad (4b)$$

where

$$\mathfrak{B}_{\{1,2\}} = \frac{E_{\{1,2\}}}{3(1 - 2\nu_{\{1,2\}})}, \quad \mathfrak{G}_{\{1,2\}} = \frac{E_{\{1,2\}}}{2(1 + \nu_{\{1,2\}})} \quad (5)$$



### 2.3 Weak form

The plate material is considered as a linearly elastic, isotropic and continuous. Based on the constitutive relations, ones obtained

$$\begin{Bmatrix} \boldsymbol{\sigma} \\ \boldsymbol{\tau} \end{Bmatrix} = \begin{bmatrix} [\mathbf{Q}^b] & [\mathbf{0}] \\ [\mathbf{0}] & [\mathbf{Q}^s] \end{bmatrix} \begin{Bmatrix} z\boldsymbol{\varepsilon} \\ \boldsymbol{\gamma} \end{Bmatrix} \quad (6)$$

where

$$\boldsymbol{\sigma} = \{\sigma_{xx} \quad \sigma_{yy} \quad \sigma_{xy}\}^T, \boldsymbol{\tau} = \{\tau_{xz} \quad \tau_{yz}\}^T \quad (7a)$$

$$\boldsymbol{\varepsilon} = \{\phi_{x,x} \quad \phi_{y,y} \quad \phi_{x,y} + \phi_{y,x}\}^T, \boldsymbol{\gamma} = \{\phi_x + w_{0,x} \quad \phi_y + w_{0,y}\}^T \quad (7b)$$

$$\mathbf{Q}^b(x, y) = \begin{bmatrix} Q_{11} & Q_{12} & 0 \\ Q_{21} & Q_{22} & 0 \\ 0 & 0 & Q_{66} \end{bmatrix}, \mathbf{Q}^s(x, y) = \begin{bmatrix} Q_{44} & 0 \\ 0 & Q_{55} \end{bmatrix} \quad (7c)$$

$$Q_{11} = Q_{22} = \frac{E(x, y)}{1-\nu^2}, Q_{12} = Q_{21} = \frac{\nu E(x, y)}{1-\nu^2}, Q_{44} = Q_{55} = Q_{66} = \frac{\kappa E(x, y)}{2(1+\nu)} \quad (7d)$$

The stress resultants are related to the strains by the following relationships

$$\{M_{\alpha\beta}, S_\alpha\} = \int_{-h/2}^{h/2} \{z\sigma_{\alpha\beta}, \tau_{\alpha z}\} dz, \{\alpha, \beta\} = \{x, y\} \quad (8)$$

From Eqs. (6) and (8),

$$\begin{Bmatrix} \mathbf{M} \\ \mathbf{S} \end{Bmatrix} = \begin{bmatrix} [\mathbf{D}^b] & [\mathbf{0}] \\ [\mathbf{0}] & [\mathbf{D}^s] \end{bmatrix} \begin{Bmatrix} z\boldsymbol{\varepsilon} \\ \boldsymbol{\gamma} \end{Bmatrix} \quad (9)$$

where  $\kappa$  is the shear correction factor, which is chosen approximately 5/6.  $D_{ij}^b(x, y) = h^3 / 12 Q_{ij}^b(x, y)$  and  $D_{ij}^s(x, y) = h Q_{ij}^s(x, y)$ .

The virtual strain energy  $\delta U$  and the virtual work done by the applied transverse distributed load  $\delta V$  are derived in detail below

$$\delta U = \int_{\Omega^e} (\delta \boldsymbol{\varepsilon}^T \mathbf{M} + \delta \boldsymbol{\gamma}^T \mathbf{S}) dx dy = \int_{\Omega^e} \delta \left\{ \boldsymbol{\varepsilon} \quad \boldsymbol{\gamma} \right\} \begin{bmatrix} [\mathbf{D}^b] & [\mathbf{0}] \\ [\mathbf{0}] & [\mathbf{D}^s] \end{bmatrix} \begin{Bmatrix} \boldsymbol{\varepsilon} \\ \boldsymbol{\gamma} \end{Bmatrix} dx dy \quad (10a)$$

$$\delta V = \int_{\Omega^e} q_0 \delta w_0 dx dy \quad (10b)$$

Now, the weak form of the plate for a typical finite element can be obtained as (Reddy 2002)

$$0 = \delta U + \delta V = \int_{\Omega^e} \delta \left\{ \boldsymbol{\varepsilon} \quad \boldsymbol{\gamma} \right\} \begin{bmatrix} [\mathbf{D}^b] & [\mathbf{0}] \\ [\mathbf{0}] & [\mathbf{D}^s] \end{bmatrix} \begin{Bmatrix} \boldsymbol{\varepsilon} \\ \boldsymbol{\gamma} \end{Bmatrix} dx dy + \int_{\Omega^e} q_0 \delta w_0 dx dy \quad (11)$$

### 3. Multi-IBFG-material topology optimization model

#### 3.1 Finite element analysis

A finite element model is built up from the afore-derived weak form. Accordingly, the generalized displacements  $\mathbf{u}$  of the  $e$ -th element are approximately expressed as

$$\mathbf{u}^h = \sum_{i=1}^4 N_i \mathbf{q}_i \quad (12)$$

where  $N_i$  is the shape functions;  $\mathbf{q} = \{w_i^0 \quad \phi_i^x \quad \phi_i^y\}^T$  is the vector of nodal displacement.

Substituting Eq. (12) into Eq. (7), the  $e$ -th element strains can be written as

$$\left\{ \boldsymbol{\varepsilon} \quad \boldsymbol{\gamma} \right\}^T = \sum_i^4 \left\{ \mathbf{B}_i^b \quad \mathbf{B}_i^s \right\}^T \mathbf{q}_i = \left\{ \mathbf{B}^b \quad \mathbf{B}^s \right\}^T \mathbf{q} \quad (13)$$

where  $\left\{ \mathbf{B}^k \right\}_{k=\{b,s\}} = \left[ \mathbf{B}_1^k \quad \mathbf{B}_2^k \quad \mathbf{B}_3^k \quad \mathbf{B}_4^k \right]$  and  $\mathbf{q}^k = \left[ \mathbf{q}_1 \quad \mathbf{q}_2 \quad \mathbf{q}_3 \quad \mathbf{q}_4 \right]$  with the strain-displacement matrices at  $i$ -th analysis node are given as

$$\mathbf{B}_i^b = \begin{bmatrix} 0 & N_{i,x} & 0 \\ 0 & 0 & N_{i,y} \\ 0 & N_{i,y} & N_{i,x} \end{bmatrix}, \quad \mathbf{B}_i^s = \begin{bmatrix} N_{i,x} & N_i & 0 \\ N_{i,y} & 0 & N_i \end{bmatrix} \quad (14)$$

### 3.2 IBFG material interpolation schemes

According to the SIMP for multiple homogeneous materials (Tavakoli and Mohseni, 2014), the relationship between Young's modulus and design variable can be expressed through the refined interpolation as follow

$$E(\rho) = \sum_{i=1}^{n+1} \rho_i^p \left[ (E_1^i - E_2^i) \left( \frac{x}{a} \right)^{k_x^i} \left( \frac{y}{b} \right)^{k_y^i} + E_2^i \right] \quad (15)$$

where  $p$  is the penalization parameter.  $n$  is the number of non-void materials.  $E_k^i$  and  $\rho_i$  denote for elastic Young's modulus of  $k$ - material component and the material phase corresponding to phase  $i$ -th.  $k_x^i$  and  $k_y^i$  stand for the power indexes in the  $x$ - and  $y$ - axis in  $k$ -th phase. Note that the refined formulation as shown in Eq. (15) returns to standard MTO when both Young's modulus components of each phase are set to be the same value, i.e.,  $E_1^i = E_2^i, \forall i$ .

### 3.3 Problem statement

Analogous to the central ideal of standard topology optimization (TO) (Bendsøe and Kikuchi 1988), MTO aims to seek the distribution of the optimum materials to attain the maximum structural stiffness for multiple materials problems. In other words, MTO becomes a minimally total strain energy problem (objective function) of the given structure with a prescribed material volume under certain constraints. The alternating active phase algorithm proposed by Tavakoli and Mohseni (2014) is applied. Based on a binary algorithm by converting the topology optimization problem of multiple materials into  $p(p-1)/2=2$  binary phase sub-problems, the multi-material topology optimization can be solved by considering only two key phases 'a' and 'b' functioning simultaneously in each subproblem (the other phases are fixed). Compared with a single material topology optimization routine, only one additional iterative loop is needed to add the current algorithm. In other words, in each subproblem of each computational step, the material properties for corresponding active phases need to be used accordingly, such as the evident formulation to an intimate relationship between two active phases 'a' and 'b' at each location may be written as follow

$$\rho_a + \rho_b = 1 - \sum_{k=1, i \neq \{a,b\}}^{n+1} \rho_k \quad (16)$$

The finite design domain  $\Omega = \sum_k \Omega_{n+1}^k$  of optimal topology problem for multiple BFG materials, as depicted in Fig. 4, is discretized into finite elements, where  $\Omega_{n+1}^k$  stands for the  $k$ -th solid and  $\Omega_{\text{void}} = \Omega_{n+1}^{n+1}$  represents the void area in multi-material problem, with  $n$  denoting the numbers of non-void materials. To avoid singularities in the equilibrium equation, a minimal lower bound non-zero value  $\varepsilon$  for design variables is used. Based on Eqs. (11),(13), (15), and (16), the general mathematical formulation of structural multi-material topology optimization problem can be stated as follows

$\begin{aligned} \text{Minimize}_{\rho_i} & : C(\mathbf{U}, \rho_i) = \mathbf{U} \mathbf{K}^T(\rho_i) \mathbf{U} \\ \text{s.t.} & : \mathbf{K}(\rho_i) \mathbf{U} = \mathbf{F} \\ & \int_{\Omega} \rho_i d\Omega \leq V_i  \Omega  \\ & 0 < \varepsilon_i \leq \rho_i \leq 1 \end{aligned}$	(17)
---	------

where  $C$  and  $\mathbf{U}$  stands for the compliance or objective function and the displacement field, respectively.  $\rho_i$  is the density vector for phase material  $i$ -th.  $V_i$  is the per-material volume fraction constraint with  $i = \overline{1, n+1}$  such that the summation should be equal to unity  $\sum_i V_i = 1$ . The discretized stiffness matrix of BFG material can be expressed as

$\mathbf{K}_{ij} = \int_{\Omega} \sum_{t=1}^{n+1} \rho_t^p \sum_{k=\{b,s\}} \gamma^t \mathbf{B}_i^{kT} \mathbf{D}_0^k \mathbf{B}_j^k d\Omega$	(18)
---	------

where the non-homogeneous parameter gamma and the nominal isotropic elasticity property matrix  $C$  corresponding to the  $k$ -th phase can be expressed as

$\gamma^t = (E_1^t - E_2^t) \left( \frac{x}{a} \right)^{k'_x} \left( \frac{y}{b} \right)^{k'_y} + E_2^t$	(19a)
--	-------

$\mathbf{D}_0^k = \frac{1}{1+\nu} \begin{bmatrix} \frac{1}{1-\nu} & \frac{\nu}{1-\nu} & 0 \\ \frac{\nu}{1-\nu} & \frac{1}{1-\nu} & 0 \\ 0 & 0 & \frac{1}{2} \end{bmatrix}$	(19b)
--	-------

in which the directional parameters can be calculated by  $\mathbf{x} = \sum_i N_i \mathbf{x}_i$ . The element strain-displacement matrices can be inscribed as

$$\mathbf{B}_i^b = \begin{bmatrix} 0 & N_{i,x} & 0 \\ 0 & 0 & N_{i,y} \\ 0 & N_{i,y} & N_{i,x} \end{bmatrix}, \quad \mathbf{B}_i^s = \begin{bmatrix} N_{i,x} & N_i & 0 \\ N_{i,y} & 0 & N_i \end{bmatrix} \quad (20)$$

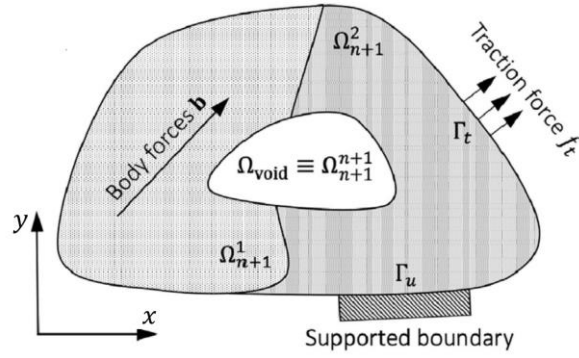


Fig. 4 Example of a multi-directional variable thickness plate

### 3.4 Assumed MITC4 shear strain field

To eliminate shear locking phenomenon in FSDT plate, the shear energy is defined in terms of the assumed covariant transverse shear strain field of the MITC4 (Bathe and Dvorkin 1985; Thompson and Thangavelu 2002). In this scheme, the membrane-bending part is approximated as a standard analysis, but the approximation of the shear strains part has to be re-defined by the linear interpolation between mid-points of the element edges, namely that assume the transversal shear interpolation in local convective coordinates to be linear in  $\eta$  direction for  $\gamma_\xi$ , and linear in  $\xi$  direction for  $\gamma_\eta$  as shown in Fig. 5.

$$\gamma_{\xi\eta} = \begin{Bmatrix} \gamma_\xi \\ \gamma_\eta \end{Bmatrix} = \frac{1}{2} \begin{Bmatrix} (1-\eta)\gamma_\xi^C + (1+\eta)\gamma_\xi^A \\ (1-\xi)\gamma_\eta^B + (1+\xi)\gamma_\eta^D \end{Bmatrix} \quad (21)$$

where the strain components at points A, B, C and D, can be directly evaluated from the displacement interpolations in Eq. (18) to obtain

$$\gamma_{\psi}^{\chi} = x_{,\psi}^{\chi} (\phi_x^a + \phi_x^b) / 2 + y_{,\psi}^{\chi} (\phi_y^a + \phi_y^b) / 2 + (w_a - w_b) / 2 \quad (22)$$

where  $(\chi, \psi, a, b) = \{(\xi, C, 2, 1), (\xi, A, 3, 4), (\eta, B, 4, 1), (\eta, D, 3, 2)\}$ .

By using MITC4 technique, the approximation of the modified shear strains components may be expressed as

$$\gamma^m = \mathbf{J}^{-T} \gamma_{\xi\eta} = \mathbf{J}^{-T} \begin{bmatrix} \gamma_{\xi\eta}^1 & \gamma_{\xi\eta}^2 & \gamma_{\xi\eta}^3 & \gamma_{\xi\eta}^4 \end{bmatrix} \mathbf{q} = \mathbf{B}^m \mathbf{q} \quad (23)$$

where

$$\gamma_{\xi\eta}^i = \begin{bmatrix} N_{i,\xi} & \xi_i x_{,\xi}^\chi N_{i,\xi} & \xi_i y_{,\xi}^\chi N_{i,\xi} \\ N_{i,\eta} & \eta_i x_{,\eta}^\psi N_{i,\eta} & \eta_i y_{,\eta}^\psi N_{i,\eta} \end{bmatrix} \quad (24)$$

in which  $(i, \chi, \psi) = \{(1, C, B), (2, C, D), (3, A, D), (4, A, B)\}$ ;  $\mathbf{J} = \partial(x, y) / \partial(\xi, \eta)$  is Jacobian transformation matrix of the mapping  $\mathbf{x} : [-1, 1]^2 \rightarrow \Omega^e$ , i.e., where  $\nabla_{\xi\eta}$  and  $\nabla$  stands for the gradient operators with respect to the  $\xi$ - $\eta$  and  $x$ - $y$  variables, respectively.

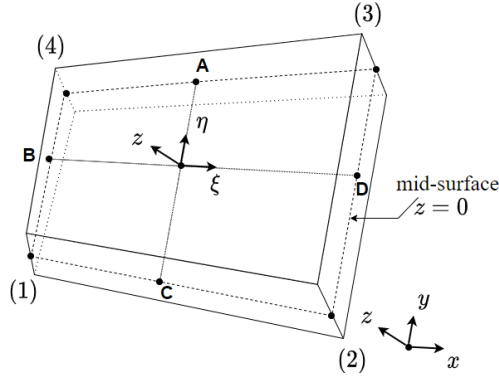


Fig. 5 Geometry of quadrilateral plate element MITC4 in the  $x$ - $y$  plane

Finally, the element stiffness matrix in Eq. (32) can be rewritten as follows.

$$\mathbf{K}_{ij} = \int_{\Omega} \sum_{t=1}^{n+1} \rho_t^p \sum_{k=\{b,m\}} \left( (E_1^t - E_2^t) \left( \frac{x}{a} \right)^{k_x^t} \left( \frac{y}{b} \right)^{k_y^t} + E_2^t \right) \mathbf{B}_i^{kT} \mathbf{D}_0^k \mathbf{B}_j^k \quad (25)$$

where  $\mathbf{B}^m = \mathbf{J}^{-T} \begin{bmatrix} \gamma_{\xi\eta}^1 & \gamma_{\xi\eta}^2 & \gamma_{\xi\eta}^3 & \gamma_{\xi\eta}^4 \end{bmatrix}$  and  $\mathbf{D}^m = \mathbf{D}^s$  are the modified derivative matrix and material property matrix of shear part, respectively.

### 3.5 Derivation of sensitivity analysis

Sensitivities of objective function  $C$  and volume  $V$  in terms of multiple non-homogeneous material densities for topology optimization can be written as by using the adjoint equation

$$\frac{\partial C}{\partial \rho_a^e} = -\mathbf{U}_e^T \frac{\partial \mathbf{K}^e}{\partial \rho_a^e} \mathbf{U}_e \quad (26a)$$

$$\frac{\partial V}{\partial \rho_a^e} = V_e \quad (26b)$$

where  $V^e$  the volume of element  $e$ . The sensitivity matrix components of each elemental stiffness for multiple non-homogeneous materials in terms of design variable of phase 'a' can be expressed as

$$\frac{\partial \mathbf{K}^e}{\partial \rho_a^e} = p \rho_a^{p-1} \sum_{t=\{a,b\}} \sum_{k=\{b,m\}} \int_{\Omega} (-1)^{\delta_{tb}} \left( (E_1^t - E_2^t) \left( \frac{x}{a} \right)^{k_x} \left( \frac{y}{b} \right)^{k_y} + E_2^t \right) \mathbf{B}_i^{kT} \mathbf{D}_0^k \mathbf{B}_j^k d\Omega \quad (27)$$

here is the density of phase 'a' at element  $e$ -th.  $\delta_{tb}$  is the Kronecker delta function of variable  $t$  and  $b$ .

#### 4. Numerical examples and discussion

In this section, several numerical tests in the analysis problem are tested to validate the proposed formulations' accuracy and applicability with the previous publication regarding analysis problems of in-plane bi-directional FG plate ( $x$ - and  $y$ - direction) (Lieu et al. 2018). The properties of IBFG materials considered in this study are listed in Table 1. In addition, three types of boundary conditions enforced throughout this study are described below (Arnold and Falk 1989):

$$\begin{aligned} \text{Hard simply supported (S}_1\text{):} & \quad \begin{cases} w_0 = \phi_y = 0 & x = 0, a \\ w_0 = \phi_x = 0 & y = 0, b \end{cases} \\ \text{Soft simply supported (S}_2\text{):} & \quad w_0 = 0 \\ \text{Clamped (C):} & \quad w_0 = \phi_x = \phi_y = 0 \end{aligned} \quad (28)$$

Table 1 Mechanical properties of FG materials

FG material		Properties	
		Young's modulus $E$ (GPa)	Poisson's ratio $\nu$
Al/Al <sub>2</sub> O <sub>3</sub> (Red) (Kumar et al. 2019)	Al <sub>2</sub> O <sub>3</sub>	380	0.3
	Al	70	0.3
Ti-6Al-4V/ZrO <sub>2</sub> (Blue) (Gouasmi et al. 2015)	ZrO <sub>2</sub>	244.27	0.3
	Ti-6Al-4V	122.56	0.3
Cu/TiB (Green) (Sobhy et al. 2015)	TiB	375	0.3
	Cu	124	0.3

##### 4.1 Verification study

An in-plane bi-directional SUS304/Si<sub>3</sub>N<sub>4</sub> square plate with  $a=b=1$  subjected to a sinusoidal load of  $q_0 \sin(\pi x/a) \cos(\pi y/a)$  is considered in the following example. Assume that the value of  $q_0$  is

set as -1, as shown in Fig. 6. Based on the Mori-Tanaka homogenization technique, the power index of  $k_x$  and  $k_y$  can express corresponding 0.0, 0.5, 1.0, and 2.0. Two kinds of boundary conditions fully clamped (CCCC) and fully hard simply supported ( $S_1S_1S_1S_1$ ) are applied. The mesh size is fixed at 50x50 for all analysis examples with the non-dimensional transverse displacement can be defined as:

$$\bar{w}_c = \frac{E_2 h^2}{a^3 q_0} w_0 \left( \frac{a}{2}, \frac{b}{2}, 0 \right) \quad (29)$$

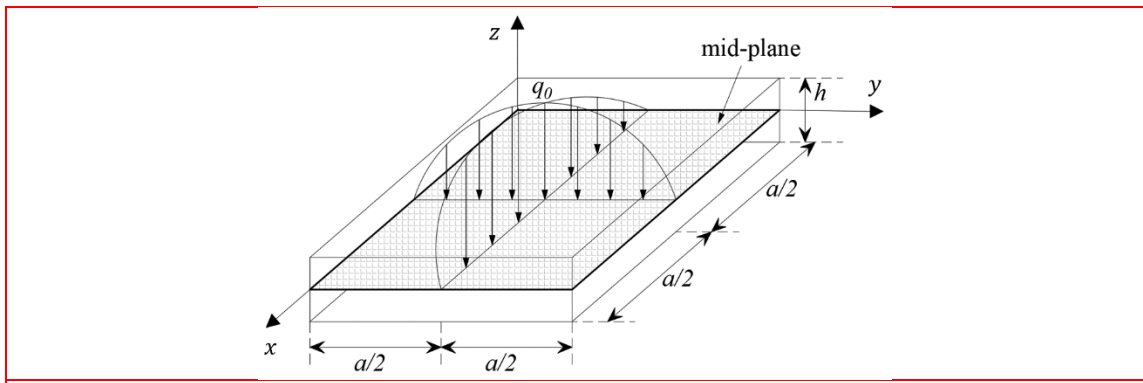


Fig. 6 Geometry of FG plate under a sinusoidally distributed load

The outcomes obtained by present solutions for all values of exponents of  $x$ - and  $y$ - directions, as exhibited in Table 2, are in good agreement with those obtained by Lieu et al. 2018 based on higher-order shear. The computed values agree well with this literature for various  $a/h$  ratios of both boundary conditions  $S_2S_2S_2S_2$  and CCCC. As can be seen, the MITC4-based FSDT model has a substantial similarity with GSDT and is free from shear-locking in case the FG plate is very thin.

Table 2 The non-dimensional deflection of in-plane bi-directional SUS304/Si<sub>3</sub>N<sub>4</sub> plate under uniform load with for different power indexes of  $x$ - and  $y$ - directions

Boundary condition	$a/h$	$k_y$	$k_x$							
			0.0		0.5		1.0		2.0	
			GSDT (Lieu et al. 2018)	FSDT						
$S_1S_1S_1S_1$	5	0.0	0.1752	0.1752	0.2075	0.2073	0.2264	0.2265	0.2485	0.2489
		0.5	0.2075	0.2073	0.2324	0.2321	0.2467	0.2466	0.2628	0.2630
		1.0	0.2264	0.2265	0.2467	0.2466	0.2579	0.2579	0.2703	0.2705
		2.0	0.2485	0.2489	0.2628	0.2630	0.2703	0.2705	0.2703	0.2785
	100	0.0	2.9039	2.9029	3.4111	3.4062	3.7074	3.7060	4.0498	4.0522
		0.5	3.4111	3.4062	3.8028	3.7961	4.0264	4.0227	4.2784	4.2780
		1.0	3.7074	3.7060	4.0264	4.0227	4.2013	4.1998	4.3945	4.3951
		2.0	4.0498	4.0522	4.2784	4.2780	4.3945	4.3951	4.5180	4.5191

CCCC	5	0.0	0.0823	0.0841	0.0983	0.1005	0.1079	0.1104	0.1191	0.1219
		0.5	0.0983	0.1005	0.1108	0.1133	0.1179	0.1206	0.1259	0.1289
		1.0	0.1079	0.1104	0.1179	0.1206	0.1235	0.1264	0.1298	0.1329
		2.0	0.1191	0.1219	0.1259	0.1289	0.1298	0.1329	0.1341	0.1372
	100	0.0	1.0346	1.0334	1.2185	1.2152	1.3239	1.3223	1.4476	1.4473
		0.5	1.2185	1.2152	1.3601	1.3557	1.4378	1.4350	1.5261	1.5246
		1.0	1.3239	1.3223	1.4378	1.4350	1.4997	1.4980	1.5691	1.5680
		2.0	1.4476	1.4473	1.5261	1.5246	1.5691	1.5680	1.6165	1.6156

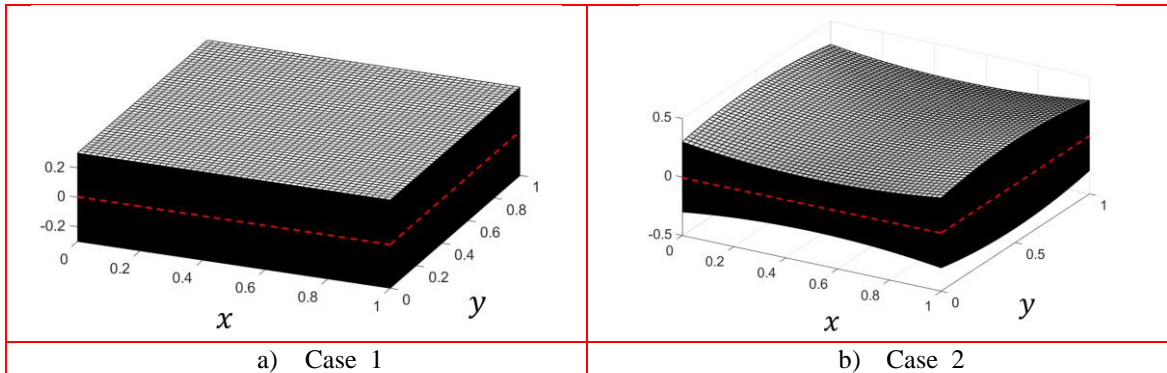
#### 4.2 The parametric study

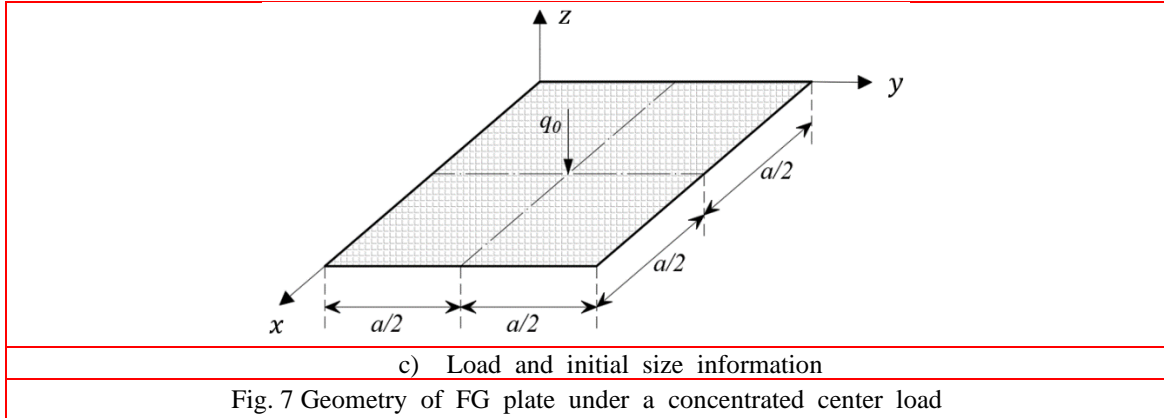
Further investigation, the influences based on the bending behavior of IBFG plate of both directions for an optimized plate design using multiple FG materials are dedicated in this part. The present study examines the change in topological and numerical FG plates' results based on each case through a prescribed volume constraint of 50%. Three boundary conditions, CCCC,  $S_1S_1S_1S_1$ , and  $S_2S_2S_2S_2$ , are considered under a concentrated load with  $q_0=-1$ , as shown in Fig. 12. A square thick IBFG steel plate with the detail mechanical properties, as defined in Table 1, are investigated in this study. The thick FG steel plate's length, width, and thickness are set  $l_x=l_y=a=1$  and  $h(x,y)$ , wherein  $h(x,y)$  can be defined into the following cases

Case 1: $h = h_0$	(30a)
-------------------	-------

Case 2: $h = h_0 \left(1 + (x - 0.5)^2 - (y - 0.5)^2\right)$	(30b)
--	-------

where  $h_0$  is set 0.3 and the filtered radius is set equal to 4.5 for all cases.



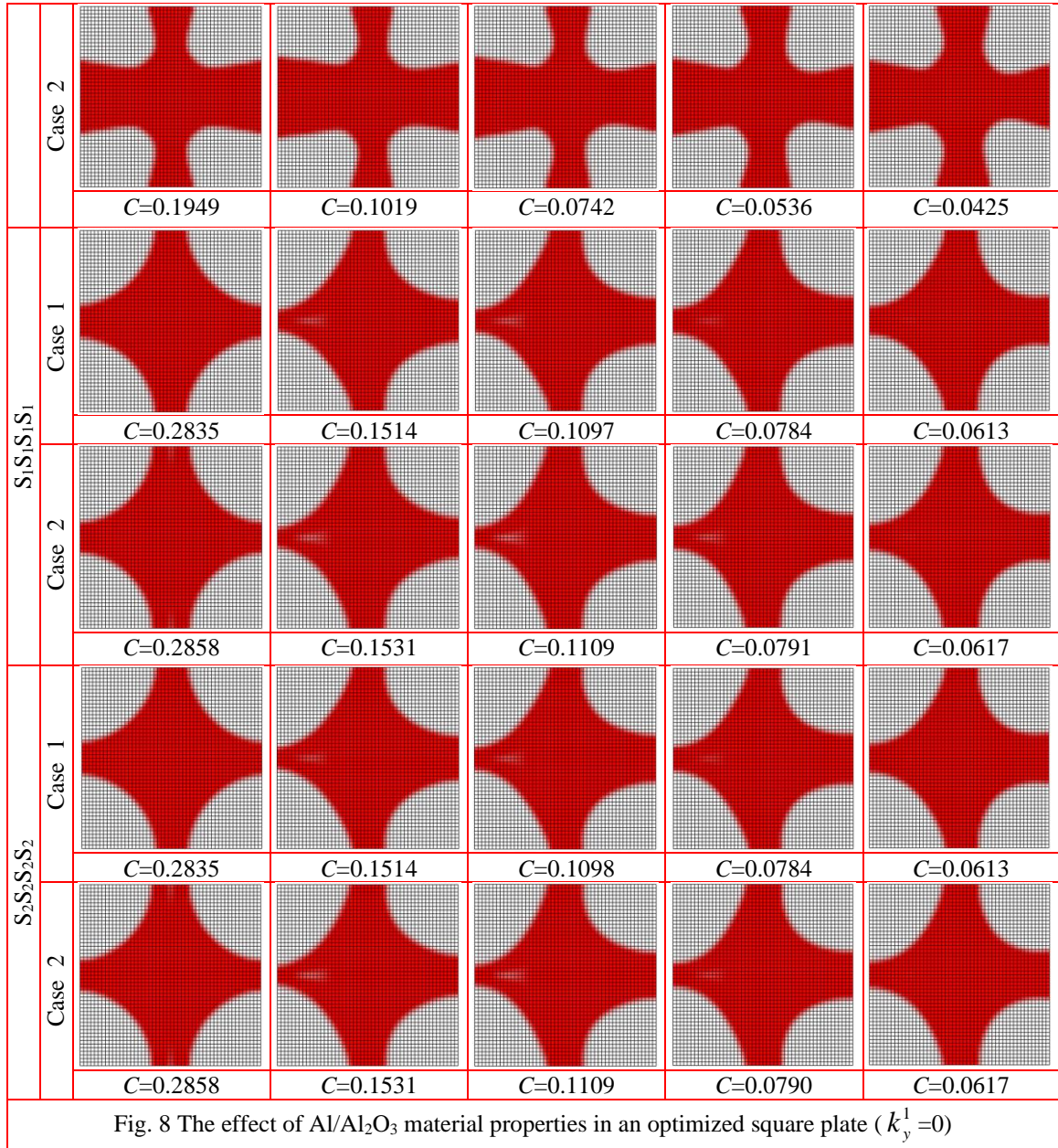


#### 4.2.1 Single IBCG material

In this part, the effect of power indexes in  $x$ -direction on the Al/Al<sub>2</sub>O<sub>3</sub> material distribution of the plate is investigated. In this part, both variable thickness function cases are considered with the different  $k_x^1=0.0-4.0$  and  $k_y^1=0$  for three boundary conditions CCCC, S<sub>1</sub>S<sub>1</sub>S<sub>1</sub>S<sub>1</sub>, and S<sub>2</sub>S<sub>2</sub>S<sub>2</sub>S<sub>2</sub>.

The optimized topology design, as depicted in Fig. 8, describes the influence of FG material properties. Overall, it is clear that the change of material distribution of CCCC tends to focus on softer material (Al) while S<sub>1</sub>S<sub>1</sub>S<sub>1</sub>S<sub>1</sub> and S<sub>2</sub>S<sub>2</sub>S<sub>2</sub>S<sub>2</sub> are distributed in a opposite side (in Al<sub>2</sub>O<sub>3</sub> side). The numerical results for FG with  $k_x^1=4.0$  were the highest compliance value, while that of other regular materials ( $k_x^1=k_y^1=0$ ) were the lowest compared with the others. Also, the ratio of FG material with  $k_x^1=4.0$  was 4.6 times higher than that of regular materials. Moreover, the compliances took in CCCC boundary condition always better than other boundary conditions. The convergence histories of the optimized topology results in all boundary conditions of both regular and FG plates ( $k_x^1=4$ ) are exhibited in Fig. 9.

B.C		$k_x^1$				
		0.0	0.5	1.0	2.0	4.0
CCCC	Case 1					
		C=0.1958	C=0.1029	C=0.0745	C=0.0534	C=0.0420



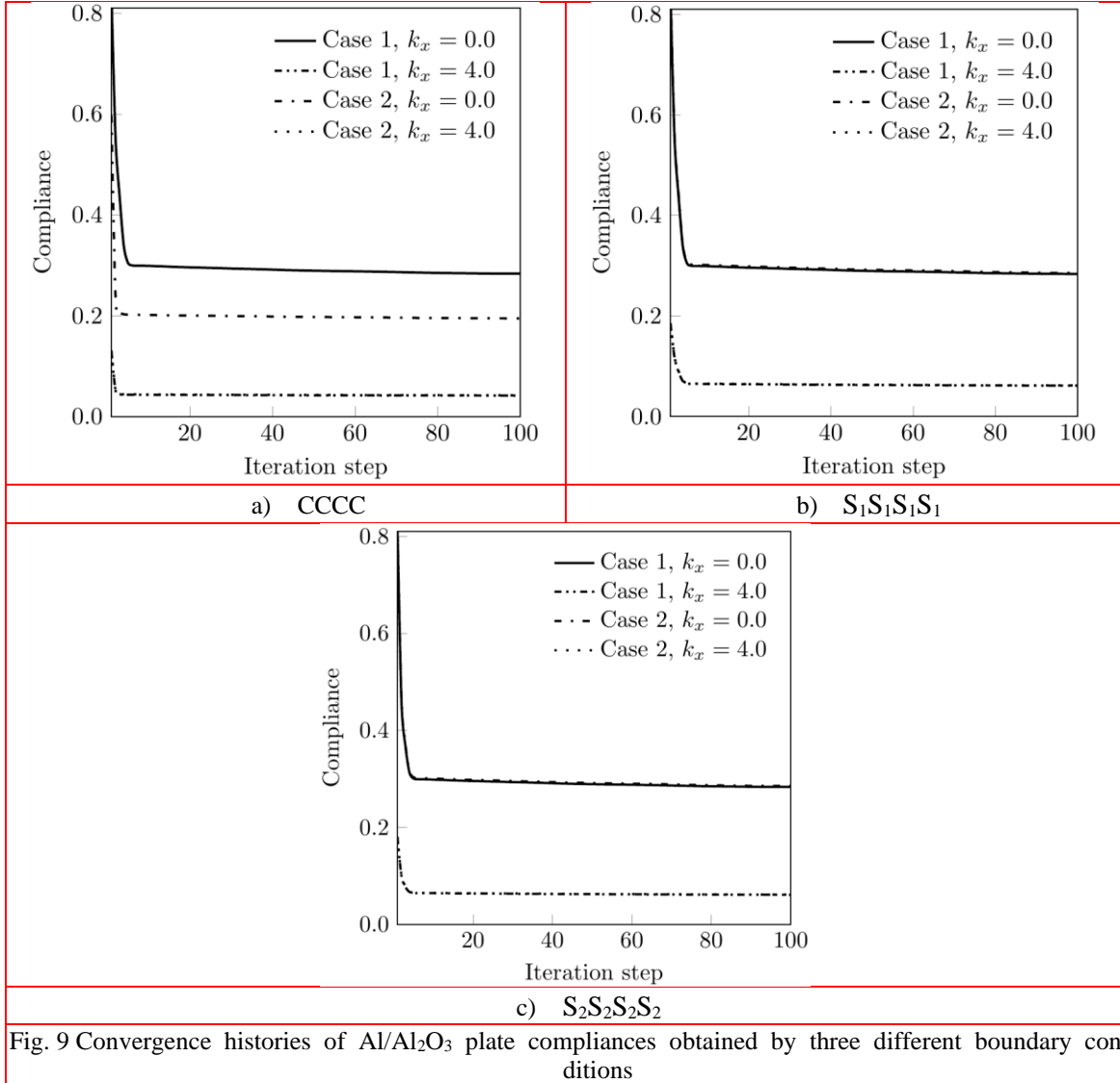


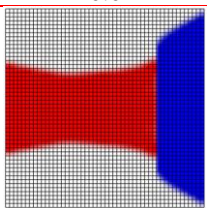
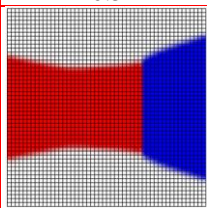
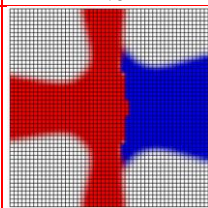
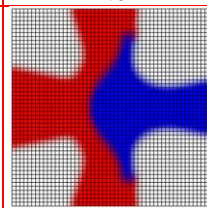
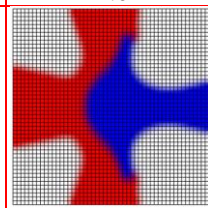
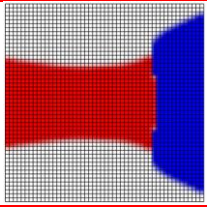
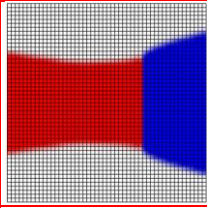
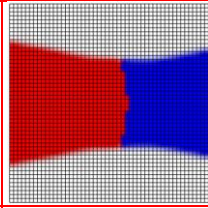
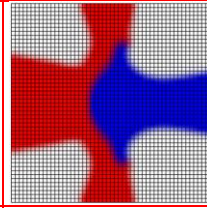
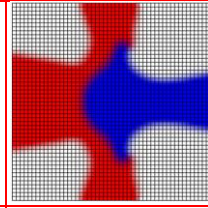
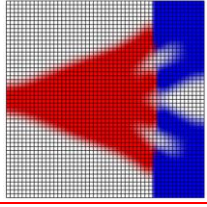
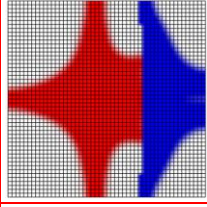
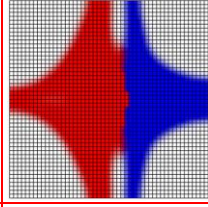
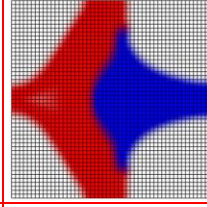
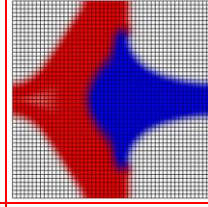
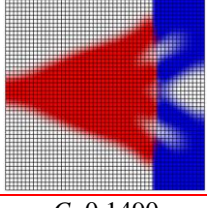
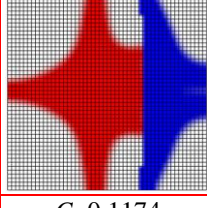
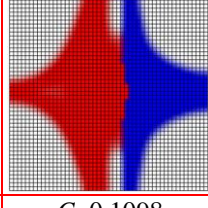
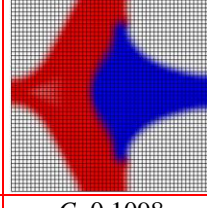
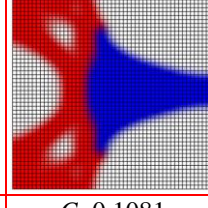
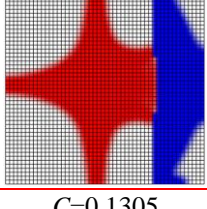
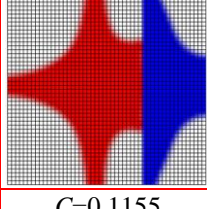
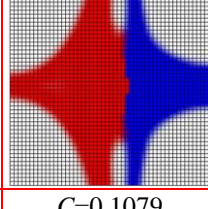
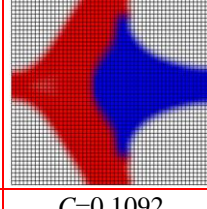
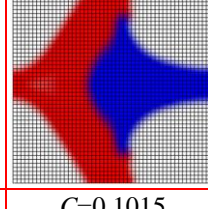
Fig. 9 Convergence histories of Al/Al<sub>2</sub>O<sub>3</sub> plate compliances obtained by three different boundary conditions

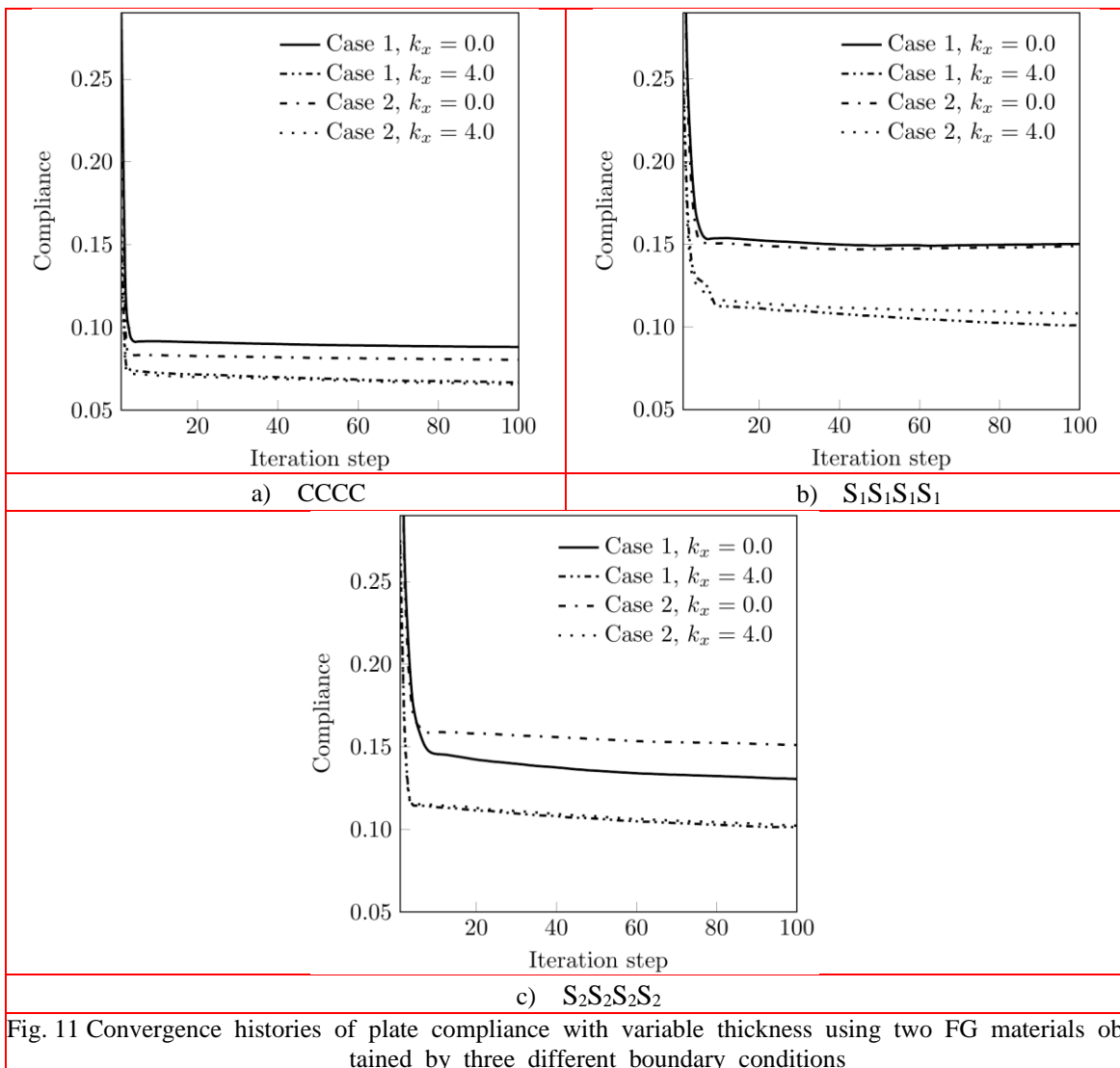
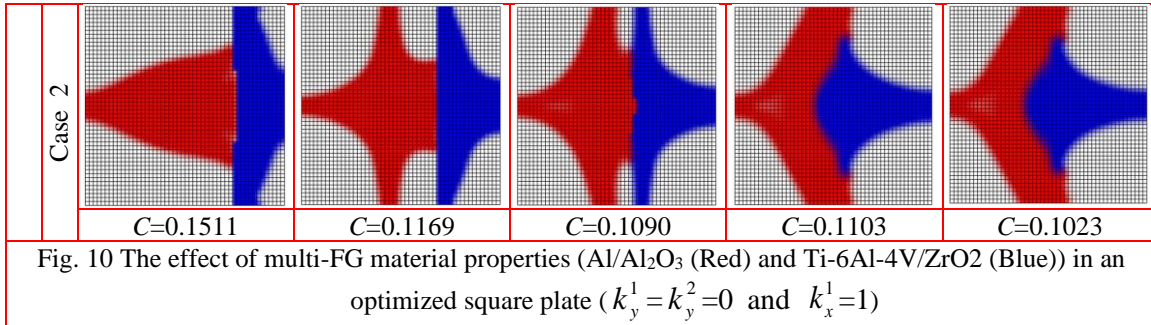
#### 4.2.2 Multiple IBFG materials

A multi-IBFG material structure that includes Al/Al<sub>2</sub>O<sub>3</sub> (Red) and Ti-6Al-4V/ZrO<sub>2</sub> (Blue) is investigated in this example. The detailed information of both FG material properties is shown in table 1. Three boundary conditions and both thickness cases with the variable power indexes  $k_x^2$  with  $k_y^1 = k_y^2 = 0$  and  $k_x^1 = 1$  are utilized.

Similar to the single material case in the previous section, the influences of optimized design using multiple FG materials into both thickness cases are depicted quite clearly. Especially in the case of the CCCC with  $k_x^2 = 1.0$  and  $S_1S_1S_1S_1$  with  $k_x^2 = 4.0$ , the optimized design in the case of

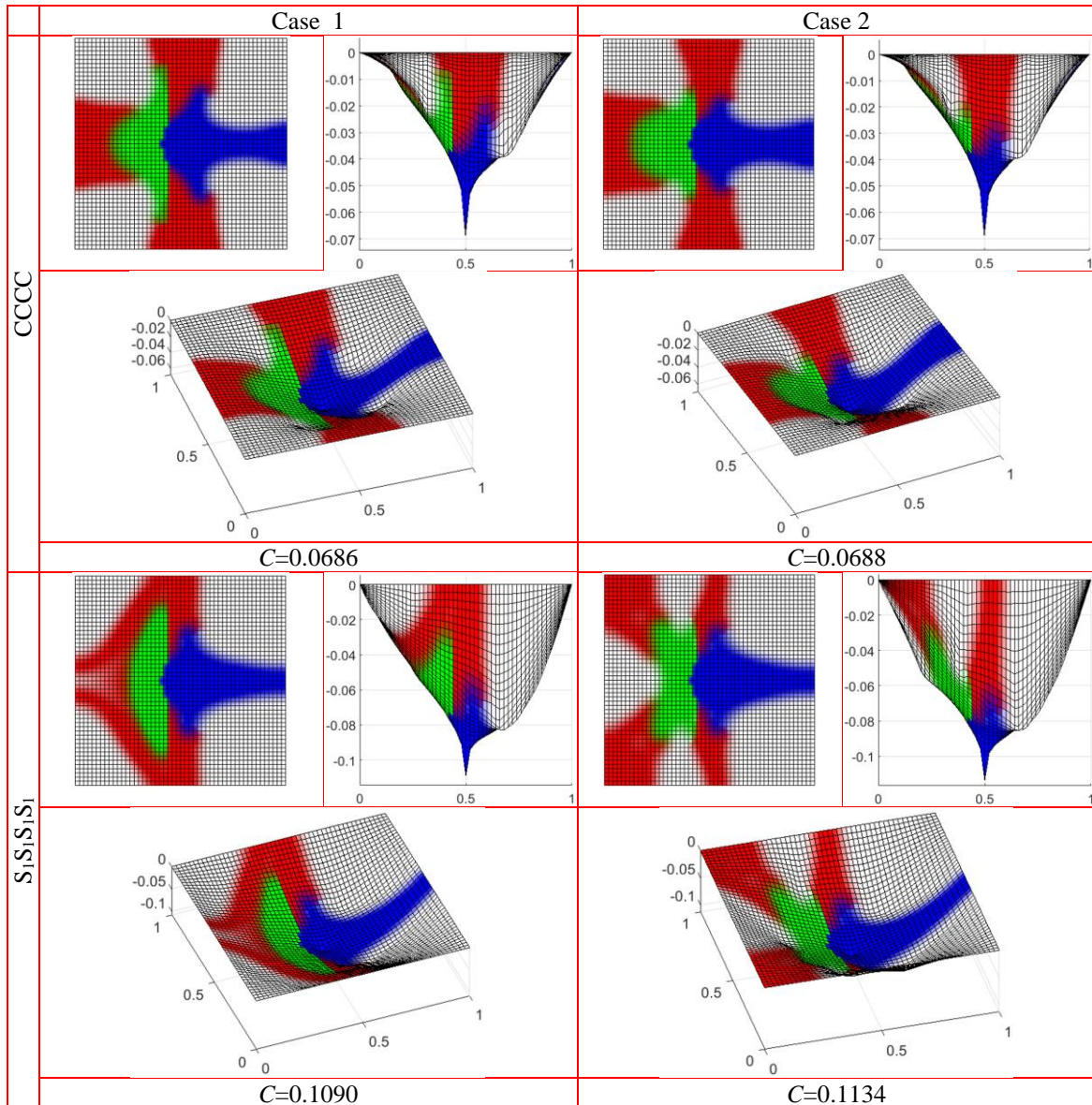
uniform thickness is different from the variable thickness case. It again demonstrates the effect of various properties of the FG material in minimizing compliance is magnificent. Moreover, due to the influence of FG material in  $S_2S_2S_2S_2$ , the impact of variable thickness in optimized design is significantly reduced. As can be seen, there is a small gap between optimized designs with different power indexes  $k_x^2$ . The convergence history of optimal compliance value of both cases with varying conditions of the boundary is shown in Fig. 11.

B.C		$k_x^2$					
		0.0	0.5	1.0	2.0	4.0	
CCCC	Case 1						
		$C=0.0882$	$C=0.0833$	$C=0.0746$	$C=0.0724$	$C=0.0667$	
	Case 2						
		$C=0.0805$	$C=0.0770$	$C=0.0751$	$C=0.0707$	$C=0.0656$	
	$S_1S_1S_1S_1$	Case 1					
			$C=0.1502$	$C=0.1158$	$C=0.1085$	$C=0.1087$	$C=0.1010$
Case 2							
		$C=0.1490$	$C=0.1174$	$C=0.1098$	$C=0.1098$	$C=0.1081$	
$S_2S_2S_2S_2$		Case 1					
			$C=0.1305$	$C=0.1155$	$C=0.1079$	$C=0.1092$	$C=0.1015$



Finally, an investigation of the influence salient properties of the multi-FG plate using three

IBFG-materials (Al/Al<sub>2</sub>O<sub>3</sub> (Red) and Ti-6Al-4V/ZrO<sub>2</sub> (Blue) and Cu/TiB (Green)) is treated. In this example, the power indexes  $k_y^1 = k_y^2 = k_y^3 = 0, k_x^1 = 1, k_x^2 = 4,$  and  $k_x^3 = 1$  are applied. Figure 12 shown the optimized and their ios-views of both cases with different boundary conditions. These results show that the stiffest material of the optimized structure tends to concentrate around load areas to meet higher stability requirements. Furthermore, the influences of variable thickness in CCCC and S<sub>2</sub>S<sub>2</sub>S<sub>2</sub>S<sub>2</sub> are almost omitted, as shown in the compliance and optimized results. The convergence histories of optimal value are shown in Fig. 13.



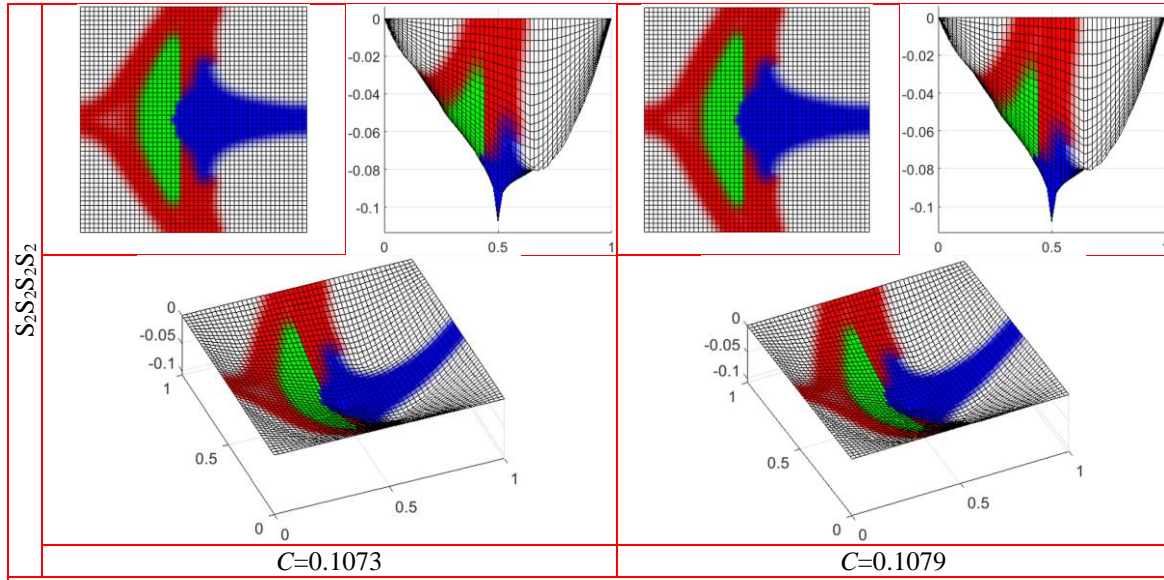


Fig. 12 The optimized design and their isos-view using multi-FG material (Al/Al<sub>2</sub>O<sub>3</sub> (Red), Ti-6Al-4V/ZrO<sub>2</sub> (Blue) and Cu/TiB (Green))

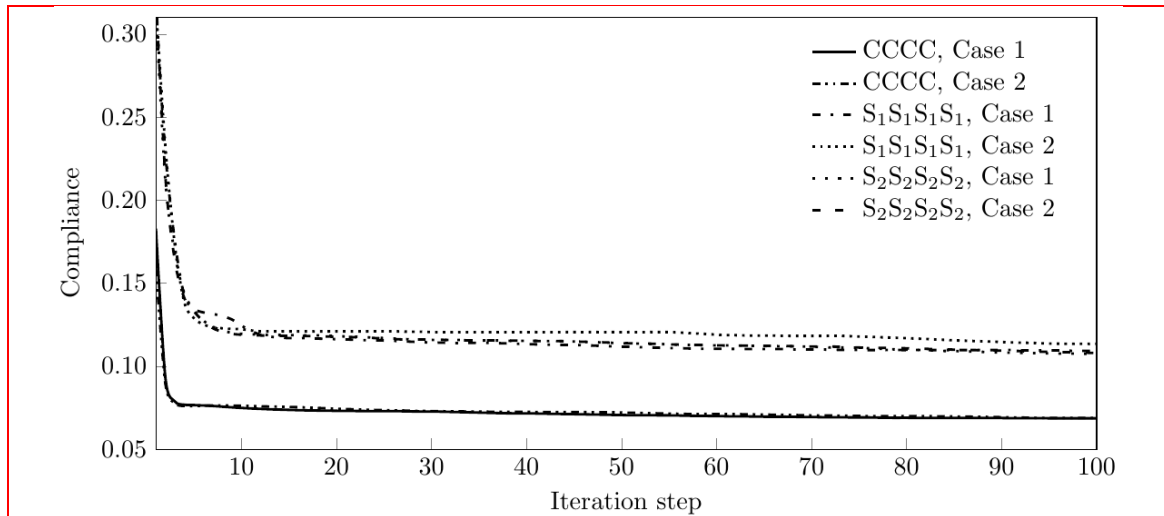


Fig. 13 Convergence histories of plate compliance with variable thickness using three FG materials obtained by three different boundary conditions

## 5. Conclusions

In this paper, an MTO using FSDT-based MITC4 of variable thickness IBFG plates is first examined for both thick and thin plates. Using specific functions, the plate thickness is continuously varied in both  $x$ - and  $y$ - directions. Furthermore, to depict the in-plane nonhomogeneous material, symmetrical volume fraction distribution of each phase is proposed. In addition, macroscopic material properties are then estimated by the Mori-Tanaka scheme. Through the present

formulations and investigated examples, several main conclusions are drawn as follows.

- (i) The IBFG Mindlin-Reissner plate is firstly considered for a structural topology optimization. Due to the problem of interactions of the elastic fields among neighboring, the Mori-Tanaka scheme is presented to create a more accurate interaction explained by the effective local bulk and shear modulus.
- (ii) Moreover, this paper is also the first effort to develop an IBFG plate for a multi-material problem. From a multi-phase TO problem with multi-volume fraction constraints, the problem is transferred into many binary phases TO sub-problems with only one volume fraction constraints. For this purpose, an alternating active-phase algorithm in conjunction with the block Gauss-Seidel method is utilized.
- (iii) The variable thickness IBFG plates based on Mindlin-Reissner plate theory with MITC4 are implemented in the MTO method. The numerical results attained by the proposed approach match well with those previously published for thick and thin plates.
- (iv) The present results can be served as benchmark solutions for future research work.

The MTO optimal topological evaluation of visualizing a mid-surface within variable thickness thick plate would be considered explicitly concerning manufacturing products. Moreover, the present mid-surface topology design with a smoothness in material boundaries may be a reasonable use of real thick and thin plates to provide the feasibility and predictability to engineers and designers.

## Acknowledgments

This research was supported by a grant (NRF-2020R1A4A2002855) from NRF (National Research Foundation of Korea) funded by MEST (Ministry of Education and Science Technology) of Korean government.

## References

- Koizumi, M. (1997), "FGM activities in Japan", *Composites Part B-Engineering*, **28**(1-2), 1-4. [https://doi.org/10.1016/S1359-8368\(96\)00016-9](https://doi.org/10.1016/S1359-8368(96)00016-9).
- Ebrahimi, F. and Salari, E. (2015), "Thermo-mechanical vibration analysis of nonlocal temperature-dependent FG nanobeams with various boundary conditions", *Composites Part B: Engineering*, **78**, 272-290. <https://doi.org/10.1016/j.compositesb.2015.03.068>.
- Şimşek, M. and Al-shujairibc, M. (2017), "Static, free and forced vibration of functionally graded (FG) sandwich beams excited by two successive moving harmonic loads", *Composites Part B: Engineering*, **108**, 18-34. <https://doi.org/10.1016/j.compositesb.2016.09.098>.
- Mantari, J.L., Ramos, I.A., Carrera, E. and Petrolo, M. (2016), "Static analysis of functionally graded plates using new non-polynomial displacement fields via Carrera Unified Formulation", *Composites Part B: Engineering*, **89**, 127-142. <https://doi.org/10.1016/j.compositesb.2015.11.025>.
- Fares, M.E., Elmarghany, M.K. and Atta, D. (2015), "The influence of the normal strain effect on the control and design optimization of functionally graded plates", *Composites Part B: Engineering*, **77**, 440-453. <https://doi.org/10.1016/j.compositesb.2015.03.003>.
- Panyatong, M., Chinnaboon, B. and Chucheepsakul, S. (2016), "Free vibration analysis of FG nanoplates embedded in elastic medium based on second-order shear deformation plate theory and nonlocal elasticity", *Composite Structures*, **153**, 428-441. <https://doi.org/10.1016/j.compstruct.2016.06.045>.
- Phung, P.V, Nguyen, T.T., Luong, H.V., Thai, C.H. and Nguyen, X.H. (2014), "A cell-based smoothed discrete shear gap method (CS-FEM-DSG3) using layerwise deformation theory for dynamic response of

- composite plates resting on viscoelastic foundation”, *Computer Methods in Applied Mechanics and Engineering*, **272**, 138-159. <https://doi.org/10.1016/j.cma.2014.01.009>.
- Nguyen, D.D and Pham, T.T. (2014), “Nonlinear response of imperfect eccentrically stiffened ceramic–metal–ceramic FGM thin circular cylindrical shells surrounded on elastic foundations and subjected to axial compression”, *Composite Structures*, **110**, 200-206. <https://doi.org/10.1016/j.compstruct.2013.11.015>.
- Mehralian, F. and Beni, Y.T. (2016), “Size-dependent torsional buckling analysis of functionally graded cylindrical shell”, *Composites Part B: Engineering*, **94**, 11-25. <https://doi.org/10.1016/j.compositesb.2016.03.048>.
- Sofiyev, A.H., Hui, D., Hacıyev, V.C., Erdem, H., Yuan, G.Q., Schnack, E. and Guldal, V. (2017), “The nonlinear vibration of orthotropic functionally graded cylindrical shells surrounded by an elastic foundation within first order shear deformation theory”, *Composites Part B: Engineering*, **116**, 170-185. <https://doi.org/10.1016/j.compositesb.2017.02.006>.
- Nemat-Alla, M. (2003), “Reduction of thermal stresses by developing two-dimensional functionally graded materials”, *International Journal of Solids and Structures*, **40**(26), 7339-7356. <https://doi.org/10.1016/j.ijsolstr.2003.08.017>.
- Tanaka, K., Tanaka, Y., Enomoto, K., Poterasu, V.F., Sugano, Y. (1993a), “Design of thermoelastic materials using direct sensitivity and optimization methods. Reduction of thermal stresses in functionally gradient materials”, *Computer Methods in Applied Mechanics and Engineering*, **106**(1-2), 271-284. [https://doi.org/10.1016/0045-7825\(93\)90193-2](https://doi.org/10.1016/0045-7825(93)90193-2).
- Tanaka, K., Tanaka, Y., Enomoto, K., Poterasu, V.F., Sugano, Y. (1993b), “An improved solution to thermoelastic material design in functionally gradient materials: Scheme to reduce thermal stresses”, *Computer Methods in Applied Mechanics and Engineering*, **109**(3-4), 377-389. [https://doi.org/10.1016/0045-7825\(93\)90088-F](https://doi.org/10.1016/0045-7825(93)90088-F).
- Tanaka, K., Watanabe, H., Sugano, Y., Poterasu, V.F., (1996), “A multicriterial material tailoring of a hollow cylinder in functionally gradient materials: Scheme to global reduction of thermoelastic stresses”, *Computer Methods in Applied Mechanics and Engineering*, **135**(3-4), 369-380. [https://doi.org/10.1016/0045-7825\(96\)01014-6](https://doi.org/10.1016/0045-7825(96)01014-6).
- Turteltaub, S. (2002a), “Functionally graded materials for prescribed field evolution”, *Computer Methods in Applied Mechanics and Engineering*, **191**(21-22), 2283-2296. [https://doi.org/10.1016/S0045-7825\(01\)00408-X](https://doi.org/10.1016/S0045-7825(01)00408-X).
- Turteltaub, S. (2002b), “Optimal control and optimization of functionally graded materials for thermomechanical processes”, *International Journal of Solids and Structures*, **39**(12), 3175-3197. [https://doi.org/10.1016/S0020-7683\(02\)00243-3](https://doi.org/10.1016/S0020-7683(02)00243-3).
- Cho, J.R. and Ha, D.Y. (2002), “Volume fraction optimization for minimizing thermal stress in Ni–Al<sub>2</sub>O<sub>3</sub> functionally graded materials”, *Materials Science and Engineering: A*, **334**(1-2), 147-155. [https://doi.org/10.1016/S0921-5093\(01\)01791-9](https://doi.org/10.1016/S0921-5093(01)01791-9).
- Chen, B. and Tong, L. (2004), “Sensitivity analysis of heat conduction for functionally graded materials”, *Materials & Design*, **25**(8), 663-672. <https://doi.org/10.1016/j.matdes.2004.03.007>.
- Chen, B. and Tong, L. (2005), “Thermomechanically coupled sensitivity analysis and design optimization of functionally graded materials”, *Computer Methods in Applied Mechanics and Engineering*, **194**(18-20), 1891-1911. <https://doi.org/10.1016/j.cma.2004.07.005>.
- Goupee, A.J. and Vel, S.S. (2006), “Two-dimensional optimization of material composition of functionally graded materials using meshless analyses and a genetic algorithm”, *Computer Methods in Applied Mechanics and Engineering*, **195**(44-47), 5926-5948. <https://doi.org/10.1016/j.cma.2005.09.017>.
- Şimşek, M. (2015), “Bi-directional functionally graded materials (BDFGMs) for free and forced vibration of Timoshenko beams with various boundary conditions”, *Composite Structures*, **133**, 968-978. <https://doi.org/10.1016/j.compstruct.2015.08.021>.
- Şimşek, M. (2016), “Buckling of Timoshenko beams composed of two-dimensional functionally graded material (2D-FGM) having different boundary conditions”, *Composite Structures*, **149**, 304-314. <https://doi.org/10.1016/j.compstruct.2016.04.034>.
- Xiang, T.S., Natarajan, S., Man, H., Song, C.M., Gao, W (2014), “Free vibration and mechanical buckling of

- plates with in-plane material inhomogeneity – A three dimensional consistent approach”, *Composite Structures*, **118**, 634-642. <https://doi.org/10.1016/j.compstruct.2014.07.043>.
- Amirpour, M., Das, R., Flores, E.I.S. (2016), “Analytical solutions for elastic deformation of functionally graded thick plates with in-plane stiffness variation using higher order shear deformation theory”, *Composites Part B: Engineering*, **94**, 109-121. <https://doi.org/10.1016/j.compositesb.2016.03.040>.
- Do, T.V., Nguyen, D.K., Duc, N.D., Doan, D.H., Bui, T.Q. (2017), “Analysis of bi-directional functionally graded plates by FEM and a new third-order shear deformation plate theory”, *Thin-Walled Structures*, **119**, 687-699. <https://doi.org/10.1016/j.tws.2017.07.022>.
- Ebrahimi, M.J. and Najafizadeh, M.M. (2014), “Free vibration analysis of two-dimensional functionally graded cylindrical shells”, *Applied Mathematical Modelling*, **38**(1), 308-324. <https://doi.org/10.1016/j.apm.2013.06.015>.
- Jalali, S.K., Naei, M.H., Poorsolhjoui, A. (2010), “Thermal stability analysis of circular functionally graded sandwich plates of variable thickness using pseudo-spectral method”, *Materials & Design*, **31**(10), 4755-4763. <https://doi.org/10.1016/j.matdes.2010.05.009>.
- Tajeddini, V., Ohadi, A., Sadighi, M. (2011), “Three-dimensional free vibration of variable thickness thick circular and annular isotropic and functionally graded plates on Pasternak foundation”, *International Journal of Mechanical Sciences*, **53**(4), 300-308. <https://doi.org/10.1016/j.ijmecsci.2011.01.011>.
- Eftekhari, S.A., Jafari, A.A. (2013), “Accurate variational approach for free vibration of variable thickness thin and thick plates with edges elastically restrained against translation and rotation”, *International Journal of Mechanical Sciences*, **68**, 35-46. <https://doi.org/10.1016/j.ijmecsci.2012.12.012>.
- Rajagopal, A. and Hodges, D.H. (2015), “Variational asymptotic analysis for plates of variable thickness”, *International Journal of Solids and Structures*, **75-76**, 81-87. <https://doi.org/10.1016/j.ijsolstr.2015.08.002>.
- Shufrin, I. and Eisenberger, M. (2016), “Semi-analytical modeling of cutouts in rectangular plates with variable thickness – Free vibration analysis”, *Applied Mathematical Modelling*, **40**(15-16), 6983-7000. <https://doi.org/10.1016/j.apm.2016.02.020>.
- Bacciocchi, M., Eisenberger, M., Fantuzzi, N., Tornabene, F., Viola, E. (2016), “Vibration analysis of variable thickness plates and shells by the Generalized Differential Quadrature method”, *Composite Structures*, **165**, 218-237. <https://doi.org/10.1016/j.compstruct.2015.12.004>.
- Javed, S., Viswanathan, K.K., Aziz, Z.A., Prabakar, K. (2016), “Free vibration of anti-symmetric angle-ply plates with variable thickness”, *Composite Structures*, **137**, 56-69. <https://doi.org/10.1016/j.compstruct.2015.11.016>.
- Zur, K.K. (2016), “Green's function for frequency analysis of thin annular plates with nonlinear variable thickness”, *Applied Mathematical Modelling*, **40**(5-6), 3601-3619. <https://doi.org/10.1016/j.apm.2015.10.014>.
- Thang, P.T., Thoi, N.T., Lee, J.H. (2016), “Closed-form expression for nonlinear analysis of imperfect sigmoid-FGM plates with variable thickness resting on elastic medium”, *Composite Structures*, **143**, 143-150. <https://doi.org/10.1016/j.compstruct.2016.02.002>.
- Bendsoe, M.P., Kikuchi, N., (1988), “Generating optimal topologies in structural design using a homogenization method. *Structural and Multidisciplinary Optimization*”, **71**, 197-224. [https://doi.org/10.1016/0045-7825\(88\)90086-2](https://doi.org/10.1016/0045-7825(88)90086-2)
- Xu, D., Chen, J., Tang, Y., Cao, J., (2012), “Topology optimization of die weight reduction for high-strength sheet metal stamping”, *International Journal of Mechanical Sciences*, **59**, 73-82. <https://doi.org/10.1016/j.ijmecsci.2012.03.006>
- Rozvany, G.I.N., Querin, O.M., Gaspar, Z., Pomezanski, V. (2002), “Extended optimality in topology design”, *Structural and Multidisciplinary Optimization* **24** (257). <https://doi.org/10.1007/s00158-002-0235-x>
- Vatanabe, S.L., Lippi, T.N., Lima, C.R., Paulino, G.H., Silva, E.C. (2016), “Topology optimization with manufacturing constraints: A unified projection-based approach”, *Advances in Engineering Software*, **100**, 97-112. <https://doi.org/10.1016/j.advengsoft.2016.07.002>.
- Roodsarabi, M., Khatibinia, M., Sarafrazi, S.R. (2016), “Hybrid of topological derivative-based level set method and isogeometric analysis for structural topology optimization”, *Steel and Composite Structures*, **21**(6), 1389-1410. <http://dx.doi.org/10.12989/scs.2016.21.6.1389>.

- Bagherinejad, M.H. and Haghollahi, A. (2018), "Topology optimization of steel plate shear walls in the moment frames", *Steel and Composite Structures*, **29**(6), 771-783. <http://dx.doi.org/10.12989/scs.2018.29.6.771>.
- Bendsøe, M.P. (1995), *Optimization of Structural Topology, Shape, and Material*, Springer-Verlag Berlin Heidelberg, Berlin, Heidelberg, Germany.
- Sigmund, O. and Torquato, S. (1997), "Design of materials with extreme thermal expansion using a three-phase topology optimization method", *Journal of the Mechanics and Physics of Solids*, **45**(6), 1037-1067. [https://doi.org/10.1016/S0022-5096\(96\)00114-7](https://doi.org/10.1016/S0022-5096(96)00114-7).
- Zhou, S.W. and Wang, M.Y., (2007), "Multimaterial structural topology optimization with a generalized Cahn–Hilliard model of multiphase transition", *Structural and Multidisciplinary Optimization*, **33**, 89. <https://doi.org/10.1007/s00158-006-0035-9>.
- Lieu, X.Q. and Lee, J.H. (2017), "A multi-resolution approach for multi-material topology optimization based on isogeometric analysis", *Computer Methods in Applied Mechanics and Engineering*, **323**, 272–302. <https://doi.org/10.1016/j.cma.2017.05.009>.
- Doan, Q.H. and Lee, D.K. (2017) "Optimum topology design of multi-material structures with nonspurious buckling constraints", *Advances in Engineering Software*, **114**, 110–120. <https://doi.org/10.1016/j.advengsoft.2017.06.002>.
- Nguyen, P.A., Banh, T.T., Lee, D.K., Lee, J.H., Kang, J., Shin, S., (2017), "Design of multiphase carbon fiber reinforcement of crack existing concrete structures using topology optimization", *Steel and Composite Structures*, **29**(5), 625-645. <http://dx.doi.org/10.12989/scs.2018.29.5.635>.
- Goo, S., Wang, S., Hyun, J., Jung, J. (2016), "Topology optimization of thin plate structures with bending stress constraints", *Computers and Structures*, **175**, 134-143. <https://doi.org/10.1016/j.compstruc.2016.07.006>.
- Belblidia, F., Lee, J.E.B., Rechak, S., Hinton, E. (2001), "Topology optimization of plate structures using a single- or three-layered artificial material model", *Advances in Engineering Software*, **32**(2), 159–168. [https://doi.org/10.1016/S0045-7949\(00\)00141-3](https://doi.org/10.1016/S0045-7949(00)00141-3).
- El-Sabbagh, A., Akl, W., Baz, A. (2008), "Topology optimization of periodic Mindlin plates", *Finite Elements in Analysis and Design*, **44**, 439-449. <https://doi.org/10.1016/J.FINEL.2008.01.016>.
- Luo, Q., Tong, L. (2017), "A deformation mechanism-based material model for topology optimization of laminated composite plates and shells", *Composite Structures*, **159**, 246-256. <https://doi.org/10.1016/j.compstruct.2016.09.056>
- Banh, T.T. and Lee, D. (2019), "Topology optimization of multi-directional variable thickness thin plate with multiple materials", *Structural and Multidisciplinary Optimization*, **59**, 1503–1520. <https://doi.org/10.1007/s00158-018-2143-8>.
- Bathe, K.J. and Dvorkin, E. (1985), "A four node plate bending element based on Mindlin-Reissner plate theory and mixed interpolation", *International Journal for Numerical Methods in Engineering*, **21**(2), 367-383. <https://doi.org/10.1002/nme.1620210213>.
- Kobayashi, H. and Sonoda, K. (1989), "Rectangular Mindlin plates on elastic foundations", *International Journal of Mechanical Sciences* **31**, 679-692. [https://doi.org/10.1016/S0020-7403\(89\)80003-7](https://doi.org/10.1016/S0020-7403(89)80003-7).
- Banh, T.T, Nguyen, Q.X., Herrmann, M., Filippou, F.C. and Lee, D.K. (2020), "Multiphase material topology optimization of Mindlin-Reissner plate with nonlinear variable thickness and Winkler foundation", *Steel and Composite Structures*, **35**(1), 129-145. <http://dx.doi.org/10.12989/scs.2020.35.1.129>.
- Senthil, S. Vel and R.C. Batra, (2002), "Exact Solution for Thermoelastic Deformations of Functionally Graded Thick Rectangular Plates" *AIAA J.*, **40**, 1421-1433. <https://doi.org/10.2514/2.1805>.
- Qian, L.F., Batra R.C. and Chen L.M., (2004), "Static and dynamic deformations of thick functionally graded elastic plates by using higher-order shear and normal deformable plate theory and meshless local Petrov–Galerkin method" *Composites Part B: Engineering*, **35**, 685-697. <https://doi.org/10.1016/j.compositesb.2004.02.004>.
- Mori T. and Tanaka K., (1973), "Average stress in matrix and average elastic energy of materials with misfitting inclusions" *Acta Metallurgica*, **21**, 571-5747. [10.1016/0001-6160\(73\)90064-3](https://doi.org/10.1016/0001-6160(73)90064-3).
- Reddy, J.N. (2002), *Energy principles and variational methods in applied mechanics*, John Wiley, New York,

NY, USA.

- Tavakoli, R. and Mohseni S., (2014), "Alternating active-phase algorithm for multimaterial topology optimization problems: a 115-line MATLAB implementation" *Structural and Multidisciplinary Optimization* volume, **49**, 621-642. <https://doi.org/10.1007/s00158-013-0999-1>.
- Thompson, L.L. and Thangavelu S.R., (2002), "A stabilized MITC element for accurate wave response in Reissner-Mindlin plates" *Computers and Structures*, **80**, 769-789.
- Lieu, X.Q., Lee, S.H., Kang, J.W., Lee, J.H., (2018), "Bending and free vibration analyses of inplane bi-directional functionally graded plates with variable thickness using isogeometric analysis", *Composite Structure*, **192**, 434-451. <https://doi.org/10.1016/j.compstruct.2018.03.021>
- Arnold, D. and R. Falk., (1989), *Analytical and Computational Models for Shells*, American Society of Mechanical Engineers, New York, New York, United States.
- Kumar, R., Lal, A., Singh B.N. and Singh, J. (2019), "Meshfree approach on buckling and free vibration analysis of porous FGM plate with proposed IHSDT resting on the foundation", *Curved and Layered Structures*, **6**(1), 192-211. [10.1515/cls-2019-0017](https://doi.org/10.1515/cls-2019-0017).
- Gouasmi, S., Megueni, A., Bouchikhi, A.S., Kamel, Z., and Abderahmane, S. (2015), "On the Reduction of Stress Concentration Factor Around a Notch Using a Functionally Graded Layer", *Materials Research*, **18**(5), 971-977. [10.1590/1516-1439.025115](https://doi.org/10.1590/1516-1439.025115).
- Sobhy, M. (2015), "Thermoelastic Response of FGM Plates with Temperature-Dependent Properties Resting on Variable Elastic Foundations", *International Journal of Applied Mechanics*, **7**(6), 1550082. <https://doi.org/10.1142/S1758825115500829>.